

# Atomic data for S II - Toward Better Diagnostics of Chemical Evolution in High-redshift Galaxies

Romas Kisielius<sup>1</sup>, Varsha P. Kulkarni<sup>2</sup>, Gary J. Ferland<sup>3</sup>, Pavel Bogdanovich<sup>1</sup>, Matt L. Lykins<sup>3</sup>

Received \_\_\_\_\_; accepted \_\_\_\_\_

---

<sup>1</sup>Institute of Theoretical Physics and Astronomy, Vilnius University, A. Goštauto 12, LT-01108, Lithuania

<sup>2</sup>Department of Physics and Astronomy, University of South Carolina, Columbia, SC 29208, USA

<sup>3</sup>Department of Physics and Astronomy, University of Kentucky, Lexington, KY 40506, USA

## ABSTRACT

Absorption-line spectroscopy is a powerful tool used to estimate element abundances in the nearby as well as distant universe. The accuracy of the abundances thus derived is, naturally, limited by the accuracy of the atomic data assumed for the spectral lines. We have recently started a project to perform the new extensive atomic data calculations used for optical/UV spectral lines in the plasma modeling code Cloudy using state-of-the-art quantal calculations. Here we demonstrate our approach by focussing on S II, an ion used to estimate metallicities for Milky Way interstellar clouds as well as distant damped Lyman-alpha (DLA) and sub-DLA absorber galaxies detected in the spectra of quasars and gamma-ray bursts (GRBs). We report new extensive calculations of a large number of energy levels of S II, and the line strengths of the resulting radiative transitions. Our calculations are based on the configuration interaction approach within a numerical Hartree-Fock framework, and utilize both non-relativistic and quasirelativistic one-electron radial orbitals. The results of these new atomic calculations are then incorporated into Cloudy and applied to a lab plasma, and a typical DLA, for illustrative purposes. The new results imply relatively modest changes ( $\approx 0.04$  dex) to the metallicities estimated from S II in past studies. These results will be readily applicable to other studies of S II in the Milky Way and other galaxies.

*Subject headings:* atomic data; atomic processes; ISM: abundances; Galaxies: abundances; quasars: absorption lines

## 1. Introduction

A powerful tool for studying distant galaxies is provided by absorption lines in the spectra of quasars superposed by foreground galaxies along the sightline, which are sampled simply by gas cross-section, independent of their brightness. Damped Lyman-alpha absorbers (DLAs; neutral hydrogen column densities  $N_{\text{HI}} \geq 2 \times 10^{20} \text{ cm}^{-2}$ ) and sub-DLAs ( $10^{19} \leq N_{\text{HI}} < 2 \times 10^{20} \text{ cm}^{-2}$ ) are especially useful for this purpose. These are the primary neutral gas reservoir for star formation at redshifts  $0 < z < 5$  [e.g., Storrie-Lombardi & Wolfe (2000); Péroux et al. (2005); Prochaska et al. (2005)]. Over the past decade, DLAs toward gamma-ray burst (GRB) afterglows have also emerged as a powerful probe of distant galaxies [e.g., Savaglio et al. (2003); Chen et al. (2005); Prochaska et al. (2007); Fynbo et al. (2009)].

The elemental compositions of DLAs/sub-DLAs offer highly sensitive tracers of the chemical evolution of galaxies [e.g., Pettini et al. (1997); Kulkarni & Fall (2002); Prochaska et al. (2003); Kulkarni et al. (2007); Prochaska et al. (2007); Péroux et al. (2008); Meiring et al. (2009); Cooke et al. (2011); Rafelski et al. (2012); Som et al. (2013)]. Element abundances in the absorbers are determined from optical/UV atomic resonance lines. Volatile elements such as N, O, P, S, Ar, Zn are not strongly condensed on interstellar dust grains; so their gas-phase abundances can give their total (gas + solid phase) abundances. In practice, for reasons such as wavelength coverage and availability of suitable lines, S and Zn have emerged as the most commonly used metallicity indicators used for DLAs. The common ionization stage of S seen in cool interstellar clouds and DLAs is S II. S II has several absorption lines that can be used to obtain reliable column densities despite their usual presence in the Lyman-alpha forest.

The accuracy of the element abundances and physical properties inferred from them depends crucially on the quality of the atomic data used. By far, the commonly used atomic

data reference for DLA spectral analysis is Morton (2003) [see, e.g., Battisti et al. (2012); Rafelski et al. (2012); Kulkarni et al. (2012); Guimaraes (2012); Jorgenson (2013); Som et al. (2013)]. For some important transitions and ions, the oscillator strengths listed in Morton (2003) have relatively large uncertainties [as listed on the NIST Atomic Spectra Database Kramida et al. (2013)], while for some transitions, oscillator strengths are not available at all. In some cases, even more recent values obtained since Morton (2003) have low accuracy grades listed in the NIST database. Limitations in atomic data can compromise our ability to read the messages received from high-redshift galaxies. To produce new reliable atomic data for commonly used astrophysical ions, we have recently started a collaborative study that brings together atomic physics, plasma simulations, and observational spectroscopy. Our goals are to assess the quality of the existing atomic data, to improve accuracy of the data that were designated low accuracies, to incorporate them into our widely used plasma simulation code Cloudy, and apply it to existing/new observations of high-redshift galaxies such as DLAs/sub-DLAs. Here we provide an early illustration of our approach by focussing on S II, an ion of great importance for DLA element abundance studies.

Being a volatile element, S does not condense easily on interstellar dust grains. In the Milky Way, S shows a depletion of  $< 0.1$  dex in cool as well as warm interstellar clouds [e.g., Savage & Sembach (1996); but see also Jenkins (2009) for the suggestion that the true depletion of S could be larger in the presence of ionization effects]. The relatively low depletion makes S ideal for estimating metallicity from gas-phase abundance measurements. Moreover, S is a fairly abundant element, so its absorption lines are easily detectable (more easily detectable than the lines of Zn, another nearly undepleted element). Especially important among the S ions is S II, which is the dominant ion in DLAs. S II has a number of absorption lines, especially a triplet at  $\lambda \lambda$  1250.6, 1253.8, 1259.5 Å, that are strong enough to be detectable. The weakest of these lines can be relatively unsaturated, giving reasonably accurate column densities (although the stronger lines can be saturated). Studies of DLAs,

especially at  $z \gtrsim 2$  often use these three S II lines to derive [S/H], and adopt that as the gas-phase metallicity. Studies of the Milky Way interstellar gas have also often adopted S as a metallicity indicator. For all of these calculations, it is naturally important to use accurate atomic data for S II.

Morton (2003) lists the oscillator strengths for the above-mentioned three S II lines to be 0.00543, 0.0109, and 0.0166, respectively, but the uncertainties in these values are classified as “C” grade, i.e. at the level of about 25% as per the NIST database. Thus, the uncertainties in the metallicity introduced by the uncertainty in the oscillator strength ( $\sim 0.1$  dex) are far larger than those often quoted from the measurement uncertainties in high-resolution data (typically  $\lesssim 0.05$  dex). S II also has absorption lines at 906.9, 910.5, and 912.7 Å, but they are too close to the Hydrogen Lyman edge and much stronger and hence likely saturated. Other S II lines at 943.0, 947.0, 1021.3, and 1021.5 Å are also listed in Morton (2003), but without oscillator strength estimates.

With the desire to assess the atomic data accuracy, we undertook new calculations of the oscillator strengths for all S II electric dipole, magnetic dipole, and electric quadrupole transitions. Section 2 describes these new calculations and compares them to previous estimates. Section 3 describes the incorporation of these calculations into Cloudy, and section 4 discusses the implications for DLA abundance studies.

## 2. Calculations of new atomic data

A broad study of energy levels, oscillator strengths and transition probabilities for the levels of some low configurations of S II was performed by Irimia & Froese Fischer (2005). The authors used multiconfiguration Hartree-Fock method (MCHF) with relativistic effects included in the Breit-Pauli approximation (BP) in their study. They have determined

all possible allowed E1 and many forbidden (E2, M1) transitions for the states under consideration and determined level lifetimes and splittings. As a first step in these calculations, *ab initio* wavefunctions were obtained, and in the next step, the diagonal energies of *LS* blocks were adjusted in order to get better agreement of the energies of *LS* terms with the observed values. We refer to the results of these calculations as MCHF<sub>05</sub>.

A following study by Froese Fischer et al. (2006) considered energy levels, lifetimes and transition probabilities for several sequences, including the S II ion as a member of P-like sequence. These authors used several theoretical methods, such as non-orthogonal spline configuration interaction, multiconfiguration Hartree-Fock, and multiconfiguration Dirac-Hartree-Fock. Transitions between the computed levels were reported for allowed E1 and some forbidden (M1, M2, E2, E3) transitions. The MCHF wavefunction expansion adopted in this work was very similar to that of Irimia & Froese Fischer (2005), but there were no term-corrections included in the Hamiltonian matrix. In the comparisons given below, we will use the results of the Froese Fischer et al. (2006) calculations as consistent configuration interaction (CI) *ab initio* calculation data and refer to them as MCHF<sub>06</sub>.

Recently, Tayal & Zatsarinny (2010) reported new calculations for transition probabilities and electron-impact collision strengths for the astrophysically important lines in S II. The multiconfiguration Hartree-Fock method with term-dependent non-orthogonal orbitals was employed for accurate representation of the target wavefunctions. Relativistic corrections were included in the Breit-Pauli approximation. Their close-coupling expansion included 70 bound levels of S II covering all possible terms of the ground  $3s^23p^3$  configuration and singly excited  $3s3p^4$ ,  $3s^23p^23d$ ,  $3s^23p^24s$ , and  $3s^23p^24p$  configurations. This approach made it possible to achieve a more accurate description of both energy levels and oscillator strengths with a relatively small CI expansion compared to that of more traditional methods with an orthogonal set of one-electron orbitals where large CI expansions are necessary.

According to Tayal & Zatsarinny (2010), the accuracy of their calculations is comparable with the accuracy of the Breit-Pauli MCHF calculations by Irimia & Froese Fischer (2005) discussed earlier. In further references, we refer to the calculations of Tayal & Zatsarinny (2010) as MCHF<sub>TD</sub>.

A systematic study of forbidden M1 and E2 transitions for P I, S II, Cl III, and Ar IV was reported by Fritzsche et al. (1999). They applied multiconfiguration Dirac-Fock (MCDF) wavefunctions of different sizes to check for the convergence of results. These authors concluded that the convergence and reasonable agreement of their calculations with previously determined results could be achieved only after a large number of valence- and core-excited configurations were included in their multiconfiguration wavefunction expansion.

The above-mentioned works are the most systematic and complex theoretical studies of allowed and forbidden transitions in S II so far. They provide more reliable line data compared to the earlier relativistic results of Mendoza & Zeippen (1982) and Keenan et al. (1993). A recent compilation by Podobedova et al. (2009) has tabulated more than 6000 allowed and forbidden lines of S I to S XV. This study provides a critical evaluation of recent theoretical values for transition rates, and also includes energy level values that are primarily experimental, taken from the NIST compilation by Kramida et al. (2013). Specifically for S II, Podobedova et al. (2009) list transition probabilities for allowed E1 transitions and forbidden M1 and E2 transitions. In this compilation, the estimated uncertainties of theoretical values in many E1 transitions exceed 25% while M1 and E2 transitions are given better accuracy.

In the present work, we employ two different approximations for the calculation of S II transition rates. In the first one, a multiconfiguration Hartree-Fock method is adopted where relativistic corrections are included in the Breit-Pauli approximation. It

resembles the method used in Froese Fischer et al. (2006), but there are several significant differences. We adopt transformed radial orbitals (TRO) (Bogdanovich 2004, 2005) in order to efficiently include electron correlation corrections caused by excited configurations with higher principal quantum numbers  $n > 4$ . In the current work, the transformed one-electron radial orbitals  $P_{\text{TRO}}(nl|r)$  have two variational parameters, an integer and even  $k$  and a positive  $B$ :

$$P_{\text{TRO}}(nl|r) = N(r^{l-l_0+k} \exp(-Br)P(n_0l_0|r) - \sum_{n' < n} P(n'l|r) \int_0^\infty P(n'l|r')r'^{(l-l_0+k)} \exp(-Br')P(n_0l_0|r')dr'). \quad (1)$$

Here the factor  $N$  ensures the normalization of the determined TROs, the first term in the parenthesis performs the transformation of RO based on the one-electron radial orbital  $P(n_0l_0|r)$  from the set of investigated configurations, and the second term ensures their orthogonality. The parameters  $k$  and  $B$  are chosen to gain the maximum of the energy correlation correction. In the current calculation, TROs were determined for the configurations with the outer electron having the principal quantum number  $5 \leq n \leq 7$  and all allowed values of the orbital quantum number  $l$ .

The second rather significant difference is in the selection of the configurations included in the CI wave function expansion. Instead of simply including higher- $n$  excited configurations, we follow the procedure described by Bogdanovich & Karpušienė (2001) and remove those configurations (admixed configurations) within the CI wavefunction expansion of the investigated configuration (adjusted configuration) which have the mean weight  $\bar{W}_{\text{PT}} < 1 \times 10^{-8}$ .

The parameter  $\bar{W}_{\text{PT}}$  is determined in the second order of perturbation theory (PT):

$$\bar{W}_{\text{PT}}(K_0, K') = \frac{\sum_{T L S T'} (2L+1)(2S+1) \langle K_0 T L S || H || K' T' L S \rangle^2}{g(K_0) (\bar{E}(K') - \bar{E}(K_0))^2}, \quad (2)$$

where  $\langle K_0 T L S || H || K' T' L S \rangle$  is a Hamiltonian matrix element for the interaction between

the adjusted  $K_0$  and the admixed  $K'$  configuration  $LS$ -terms,  $g$  is the statistical weight of the configuration  $K_0$ , and  $\bar{E}$  are the averaged energies of the configurations. This method, paired with the methods from Bogdanovich et al. (2002), makes it possible to significantly reduce the size of the Hamiltonian matrices.

In the CI approximation, our methods allow for the use of two kinds of radial orbitals describing the electrons of adjusted configurations which are applied for the transformations (1). In the case of S II, we have electrons with the principal quantum number  $n \leq 4$ . Traditionally, the solutions of the standard Hartree-Fock equations are utilized for this purpose, see, e.g. Bogdanovich et al. (2003); Jonauskas et al. (2005, 2006); Karpušienė & Bogdanovich (2009). We use the notation  $CI_{\text{HF+TRO}}$  to denote the results obtained for this approximation. Relativistic corrections are included in the Breit-Pauli approximation, as in the MCHF calculations.

In order to partially account for relativistic corrections at the stage when the one-electron radial orbitals are determined, we developed a new method which solves the quasirelativistic (QR) Hartree-Fock equations. The quasirelativistic radial orbitals, obtained after solving the QR equations, are applied to determine the one-electron wavefunctions of admixed configurations and further to calculate the transformed radial orbitals given by Eq. 1. A consequent inclusion of correlation effects is achieved by the same method as in the case of the afore-mentioned non-relativistic Hartree-Fock radial orbitals. To determine the energy levels, the Breit-Pauli approximation is applied as in the  $CI_{\text{HF+TRO}}$  calculations. We use the  $CI_{\text{QR+TRO}}$  notation for this method. Furthermore, we must mention that our QR method differs significantly from the more traditional quasirelativistic method of Cowan (1981). A more detailed description of the applied QR approximation can be found elsewhere [see, e.g., Bogdanovich & Rancova (2006, 2007, 2008); Bogdanovich & Kisielius (2012, 2013)].

### 3. Accuracy of atomic data sets

One the main tasks of the present paper is to assess the accuracy of the spectroscopic data used in modeling the S II emission or absorption spectra. In order to do that, we compare our results, both in the  $CI_{\text{HF}+\text{TRO}}$  and  $CI_{\text{QR}+\text{TRO}}$  approximations, with those from Froese Fischer et al. (2006) and Tayal & Zatsarinny (2010) calculations.

#### 3.1. Energy levels and wavelengths

Table 1 presents the energy levels of S II. The results of our calculations obtained with the two methods are compared with the experimental data and with the values calculated by Froese Fischer et al. (2006) and Tayal & Zatsarinny (2010). One can see from the mean-square deviations (*MSD*) provided at the bottom of Table 1 that the data of Tayal & Zatsarinny (2010) agree with the experimental values better than with both sets of our data or those of Froese Fischer et al. (2006), although the differences among calculated values are rather small. The better accuracy of the Tayal & Zatsarinny (2010) data can be explained by the fact that those authors used the term-dependent non-orthogonal radial orbitals to calculate energy levels and radiative transition parameters. Such an approximation determines the eigenvalues for each *LS*-term separately instead of optimizing a complete set of terms.

Nevertheless, some deviations in energy level values (consequently, in transition wavelength values) are not significant, and they do not exceed 3%. Moreover, these discrepancies can be overcome by using the experimental wavelengths, which are well-known for the most important S II lines, for the line identification or by using the experimental energy differences to determine the “corrected” oscillator strengths or radiative transition probabilities [see Verner et al. (1996)].

Table 1. Comparison of calculated S II energy levels with experimental data.

$N$	State	$J$	CI <sub>HF+TRO</sub>	CI <sub>QR+TRO</sub>	Exp	MCHF <sub>06</sub>	MCHF <sub>TD</sub>
1	$3p^3 \ ^4S$	1.5	0	0	0	0	0
2	$3p^3 \ ^2D$	1.5	15292	15320	14853	15282	14880
3	$3p^3 \ ^2D$	2.5	15307	15335	14885	15311	14905
4	$3p^3 \ ^2P$	0.5	25407	25549	24525	24817	24632
5	$3p^3 \ ^2P$	1.5	25431	25574	24572	24848	24656
6	$3s3p^4 \ ^4P$	2.5	77787	78926	79395	78468	79405
7	$3s3p^4 \ ^4P$	1.5	78106	79249	79757	78763	79704
8	$3s3p^4 \ ^4P$	0.5	78290	79434	79963	78929	79873
9	$3s3p^4 \ ^2D$	2.5	97281	98322	97919	97500	97875
10	$3s3p^4 \ ^2D$	1.5	97284	98324	97891	97481	97899
11	$3p^23d \ ^2P$	1.5	105241	105702	105599	105444	105530
12	$3p^23d \ ^2P$	0.5	105599	106062	106044	105846	105933
13	$3p^24s \ ^4P$	0.5	109399	109344	109561	108939	109635
14	$3p^24s \ ^4P$	1.5	109600	109548	109832	109182	109877
15	$3p^24s \ ^4P$	2.5	109927	109880	110269	109570	110264
16	$3p^23d \ ^4F$	1.5	110068	110275	110177	110174	110216
17	$3p^23d \ ^4F$	2.5	110179	110387	110313	110297	110337
18	$3p^23d \ ^4F$	3.5	110336	110547	110509	110473	110514
19	$3p^23d \ ^4F$	4.5	110543	110757	110767	110705	110748
20	$3p^24s \ ^2P$	0.5	113060	113029	112938	112487	113055
21	$3p^24s \ ^2P$	1.5	113449	113422	113462	112952	113514
22	$3p^23d \ ^4D$	0.5	113864	114082	114162	113986	114144
23	$3p^23d \ ^4D$	1.5	113896	114115	114201	114020	114176
24	$3p^23d \ ^4D$	2.5	113940	114160	114231	114064	114216
25	$3p^23d \ ^4D$	3.5	113996	114216	114279	114120	114265
26	$3p^23d \ ^2F$	2.5	114942	115190	114804	115018	114853
27	$3p^23d \ ^2F$	3.5	115310	115563	115286	115437	115281
28	$3s3p^4 \ ^2S$	0.5	119175	119904	119784	119887	119862
29	$3p^24s \ ^2D$	1.5	121656	121612	121529	121230	121499
30	$3p^24s \ ^2D$	2.5	121658	121614	121530	121230	121499
31	$3p^23d \ ^2G$	3.5	127320	127489	127127	127771	127161
32	$3p^23d \ ^2G$	4.5	127332	127501	127128	127773	127161
33	$3p^23d \ ^4P$	2.5	131737	132161	130602	131100	130775
34	$3p^23d \ ^4P$	1.5	131913	132343	130819	131292	130960
35	$3p^23d \ ^4P$	0.5	132019	132452	130949	131406	131073
36	$3p^23d \ ^2D$	1.5	134648	135023	133361	133915	133469
37	$3p^23d \ ^2D$	2.5	135065	135454	133815	134346	133864
38	$3p^24s \ ^2S$	0.5	136559	136753	136329	136026	136315
39	$3p^23d \ ^2P$	0.5	140742	140939	139845	140485	139881
40	$3p^23d \ ^2P$	1.5	140826	141021	140017	140667	140034
41	$3p^23d \ ^2F$	3.5	141879	142499	138527	139950	138639
42	$3p^23d \ ^2F$	2.5	141896	142516	138509	139956	138614
43	$3p^23d \ ^2D$	2.5	145843	146418	144009	144982	144308
44	$3p^23d \ ^2D$	1.5	146011	146599	144142	145138	144422
45	$3s3p^4 \ ^2P$	1.5	152020	153750	145506	145933	145631
46	$3s3p^4 \ ^2P$	0.5	152326	153955	145878	146418	145946
47	$3p^23d \ ^2D$	2.5	152340	153207	148887	150450	149067
48	$3p^23d \ ^2D$	1.5	152491	153257	148901	150614	149075
49	$3p^23d \ ^2S$	0.5	154834	155791	151652	153365	151745
<i>MSD</i>			1710	2071	–	698	94

Note. — CI<sub>HF+TRO</sub> - our HF data; CI<sub>QR+TRO</sub> - our quasirelativistic data; Exp - experimental values; MCHF<sub>06</sub> - data from Froese Fischer et al. (2006); MCHF<sub>TD</sub> - data from Tayal & Zatsarinny (2010).

### 3.2. E1 lines

We have determined radiative transition parameters for the lines arising from the transitions among the levels of  $3s^23p^3$ ,  $3s3p^4$ ,  $3p^23d$ , and  $3p^24s$  configurations of S II. The electric dipole, electric quadrupole and magnetic dipole transitions were considered. The main target of the present work is not only to determine high-accuracy radiative transition data but also to evaluate the accuracy of the calculations and their suitability for use in the plasma modeling code Cloudy.

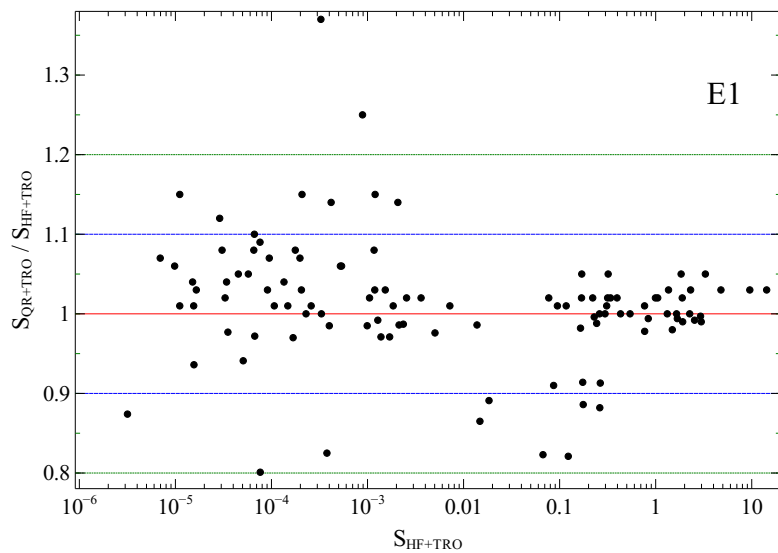


Fig. 1.— Comparison of the E1 transition line strengths  $S$  determined in the  $CI_{HF+TRO}$  and  $CI_{QR+TRO}$  approaches for S II.

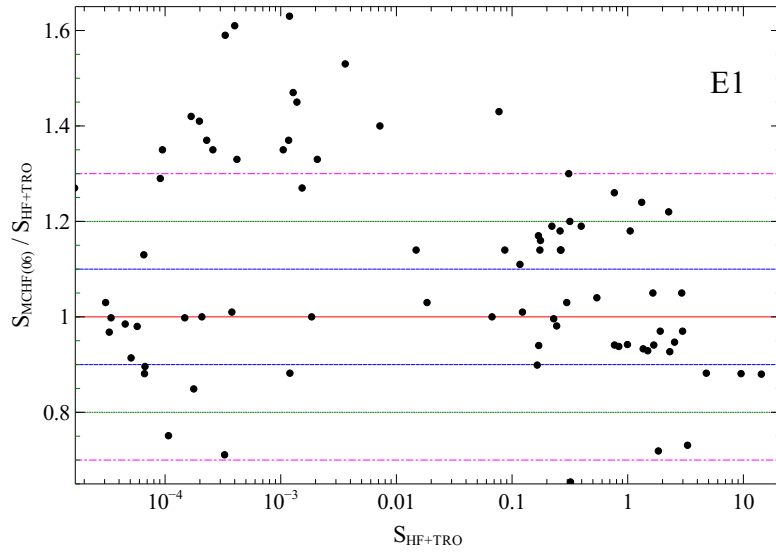


Fig. 2.— Comparison of the E1 transition line strengths  $S$  determined in the  $\text{CI}_{\text{HF+TRO}}$  and  $\text{MCHF}_{06}$  (Froese Fischer et al. 2006) approaches for S II.

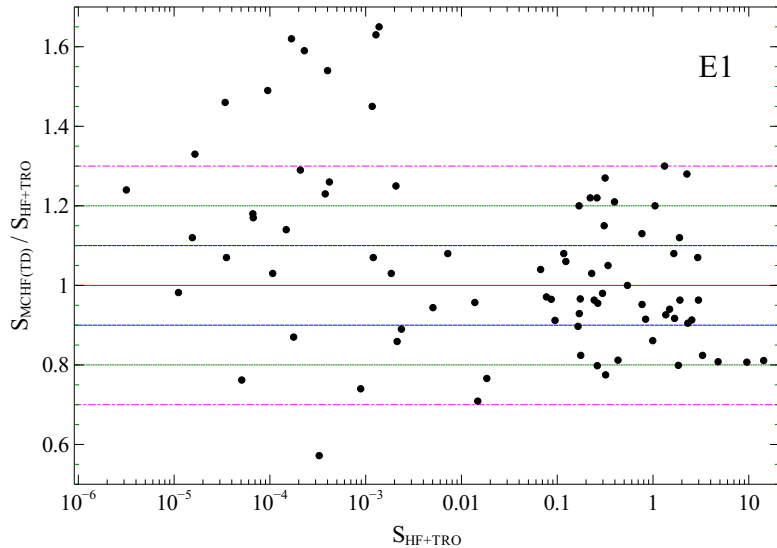


Fig. 3.— Comparison of the E1 transition line strengths  $S$  determined in the  $\text{CI}_{\text{HF}+\text{TRO}}$  and  $\text{MCHF}_{\text{TD}}$  (Tayal & Zatsarinny 2010) approaches for S II.

One of the ways to assess the accuracy of our results is to compare them with other available data. For this purpose we make a comparison of the E1 transition line strengths  $S$ . Transition line strengths  $S$  are chosen, because they do not depend directly on the transition energy difference, unlike the oscillator strengths  $f$  or transition probabilities  $A$ . As it is mentioned before, the accuracy of  $f$ -values and  $A$ -values can be increased by using theoretically calculated  $S$ -values and the experimental transition energy or the wavelength  $\lambda$ .

Figure 1 compares our calculated results determined using two different approximations. The  $\text{CI}_{\text{HF}+\text{TRO}}$  approach utilizes non-relativistic radial orbitals while the  $\text{CI}_{\text{QR}+\text{TRO}}$  approach employs quasirelativistic radial orbitals. These two approaches adopt the same configuration interaction method, involving the transformed radial orbitals, to deal with the correlation effects. As one can see, agreement of the results is rather nice, especially for the strongest lines. Within 2 orders of magnitude, the discrepancies do not exceed 10%, except for 3 lines. Within 4 orders of magnitude, the most discrepancies are within 10%, but there are 5 more

lines with the discrepancies ranging from 10% to 20%. Extending comparison to 6 orders of magnitude, situation does not change substantially, and the most lines agree within 10%. Nevertheless, there are some lines where discrepancies exceed 20% or even 30%.

Comparison of our  $CI_{\text{HF+TRO}}$  calculation results with the data from Froese Fischer et al. (2006) is given in Fig. 2. As one can see, the agreement of these data is worse in Fig. 2, as compared to Fig. 1. This is caused by the use of different CI expansion bases in our and Froese Fischer et al. (2006) calculations. In general, the discrepancies for most of the strong lines are within 20% except for the few lines with the discrepancies larger than that, when transition line strengths within 3 orders of magnitude are considered. One can see some larger deviations, exceeding 30% in this comparison but the number of such lines is small. For weaker lines, there is a large number of lines with discrepancies exceeding 30%.

In Fig. 3, a similar comparison of our  $CI_{\text{HF+TRO}}$  results with the data from Tayal & Zatsarinny (2010) is presented. Here again, the discrepancies do not exceed 30% and in most cases are below 20% for the line strength range of 4 orders of magnitude. There are just 5 lines with discrepancies exceeding 25%. When weaker lines are considered, agreement of data resulting from different approximations is worse, and in some cases, the discrepancies can reach 50% or even more.

We conclude that our two sets of calculations for the radiative transition data agree very well between themselves for the strongest transitions, within 6 orders of magnitude of the largest line strengths. This proves that relativistic corrections are included adequately in our  $CI_{\text{HF+TRO}}$  approximation. For the weakest lines, where transitions purely depend on configuration interaction effects, this close agreement breaks down even if the CI basis remains the same. Comparison with the data from Froese Fischer et al. (2006) and Tayal & Zatsarinny (2010) demonstrates, that, for the strongest lines, deviations are within 20% to 30% for the line strengths varying by 4 orders of magnitude from the strongest. Agreement

for many weaker lines is worse and exceeds 30%, as the above-mentioned studies apply different CI bases compared to our calculations.

The particular S II lines listed in Table 2 were chosen because they are all of the lines from S II listed by Morton (2003), which is the commonly used reference in observational spectroscopy of quasar absorption systems and Galactic interstellar medium. The most commonly used lines are the triplet at 1250.578, 1253.805, 1259.518 Å, as they have determinations of oscillator strengths and are relatively easy to observe being longward of the H I Lyman- $\alpha$  transition, and often outside the red wing of the Lyman- $\alpha$  transition. The doublets at or below 912 Å are difficult to observe due to their proximity to the H I Lyman limit. In the case of DLA/sub-DLAs (and in general the Lyman-limit systems), absorption near the H I Lyman limit renders the quasar flux to be nearly zero in this wavelength region. Nevertheless, we list them in Table 2 for the sake of completeness. The doublets at 1021.254, 1021.539 Å and at 943.003, 946.978 Å can in principle be observed with more ease, but have no measurements of oscillator strengths listed in Morton (2003). From our calculations for these lines as well as those from other works presented in Table 2, it is clear that observing these lines will be far more challenging. But the strongest of these lines (at 1021.539 Å) may be possible to detect in the strongest absorbers. For example, in a solar-metallicity absorber with  $\log N_{\text{HI}} = 22.0$ , the S II  $\lambda$  1021.254 line would be expected to have a rest-frame equivalent width of  $\approx 12$  mÅ.

In the last column of Table 2 we present the  $gf$ -values for these lines. These values are derived from the line strengths  $S$  calculated in the  $\text{CI}_{\text{HF+TRO}}$  approximation with the experimentally adjusted transition energies. We give oscillator strengths as the product  $gf$  due to its symmetry. We note that the emission  $f_{u,l}$  and absorption  $f_{l,u}$  values are related by  $g_u f_{u,l} = -g_l f_{l,u}$ . The lines originating from the excited  $3p^2(^3P)3d^2P_{3/2}$  and  $3p^2(^3P)3d^2P_{1/2}$  levels (at 943.003, 946.978 Å) are very weak. For them we find the largest discrepancies

Table 2. Comparison of calculated transition rates  $A$  ( $\text{s}^{-1}$ ) for some E1 transitions to the ground state  $3p^3\ ^4S_{3/2}$ .

Excited state	$\lambda_{\text{Exp}}(\text{\AA})$	$ag$	$\text{CI}_{\text{HF+TRO}}$	$\text{CI}_{\text{QR+TRO}}$	$\text{MCHF}_{\text{TD}}$	$\text{MCHF}_{06}$	$\text{MCHF}_{05}$	$gf^{\text{corr}}$
$3s3p^4\ ^4P_{5/2}$	1259.518	$D+$	4.48E+7	4.02E+7	4.27E+7	4.92E+7	5.10E+7	6.27E-2
$3s3p^4\ ^4P_{3/2}$	1253.805	$D+$	4.48E+7	4.00E+7	4.30E+7	4.93E+7	5.10E+7	4.14E-2
$3s3p^4\ ^4P_{1/2}$	1250.578	$D$	4.48E+7	4.00E+7	4.32E+7	4.94E+7	5.11E+7	2.06E-2
$3s3p^4\ ^2D_{5/2}$	1021.254	$ng$	3.41E+4	3.47E+4	3.50E+4	2.51E+4	2.61E+4	3.17E-5
$3s3p^4\ ^2D_{3/2}$	1021.539	$ng$	5.28E+3	5.40E+3	5.17E+3	3.54E+3	3.67E+3	3.28E-6
$3p^2(^3P)3d\ ^2P_{3/2}$	946.978	$ul$	2.42E+2	1.49E+3	4.24E+3	2.68E+3	2.10E+3	8.02E-7
$3p^2(^3P)3d\ ^2P_{1/2}$	943.003	$ul$	9.87E+1	1.08E+3	9.45E+2	1.20E+3	7.65E+2	2.88E-7
$3p^2(^3P)4s\ ^4P_{1/2}$	912.735	$D+$	1.12E+9	1.10E+9	1.02E+9	1.03E+9	1.05E+9	2.78E-1
$3p^2(^3P)4s\ ^4P_{3/2}$	910.484	$C$	1.13E+9	1.11E+9	1.03E+9	1.04E+9	1.06E+9	5.60E-1
$3p^2(^3P)4s\ ^4P_{5/2}$	906.885	$C$	1.15E+9	1.13E+9	1.05E+9	1.07E+9	1.08E+9	8.49E-1

Note. — Transition wavelengths  $\lambda_{\text{exp}}$  are experimental values.  $\text{CI}_{\text{HF+TRO}}$  - our MCHF data adjusted for the experimental transition energies;  $\text{CI}_{\text{QR+TRO}}$  - our quasirelativistic Hartree-Fock data;  $\text{MCHF}_{\text{TD}}$  - data from Tayal & Zatsarinny (2010);  $\text{MCHF}_{06}$  - data from Froese Fischer et al. (2006);  $\text{MCHF}_{05}$  - data from Irimia & Froese Fischer (2005).  $gf^{\text{corr}}$  are “corrected”  $gf$  values based on our calculations adjusted for the experimental transition energies. Accuracy grades  $ag$  are taken from Kramida et al. (2013),  $C$  means assumed 25% accuracy,  $D$  means assumed 40% accuracy,  $D+$  means assumed 50% accuracy,  $ng$  means no accuracy grade is given,  $ul$  means lines are not listed in Kramida et al. (2013).

when different data sets are compared. Unfortunately, our  $CI_{\text{HF+TRO}}$  results do not agree very well with other data, therefore  $gf^{\text{corr}}$  values for these two lines were derived from our  $CI_{\text{QR+TRO}}$  calculations which are in much better agreement with the data from Tayal & Zatsarinny (2010) and Froese Fischer et al. (2006).

### 3.3. E2 and M1 lines

The line strengths  $S$  of E2 transitions from our two sets of calculations are compared in Fig. 4. As one can see, the deviations do not exceed 20%, except for a few weaker lines. But even for these lines, the deviations are smaller than 30%. Moreover, the deviations for most of the lines are  $< 10\%$ . So here again, our two calculation methods,  $CI_{\text{HF+TRO}}$  and  $CI_{\text{QR+TRO}}$ , produce very similar results.

A comparison of our  $CI_{\text{HF+TRO}}$  results with the data from Froese Fischer et al. (2006) is shown in Fig. 5. It is evident that the scatter in the ratio  $S_{\text{MCHF}_{06}}/S_{\text{CI}_{\text{HF+TRO}}}$  is significantly larger compared to the scatter in the  $S_{\text{CI}_{\text{QR+TRO}}}/S_{\text{CI}_{\text{HF+TRO}}}$  ratio. Nevertheless, the lines within 2 orders of magnitude of the strongest have deviations smaller than 20%, while most of the remaining weaker lines have deviations smaller than 30%. We note that there are some rather strong lines ( $0.1 \leq S \leq 1$ ), which have deviations  $> 30\%$  or even  $> 40\%$ . But the total number of lines having deviations larger than 30% is around 20.

Figure 6 compares our calculated line strengths for the M1 transitions. As one can see, the agreement is very good. For almost all the lines, the two values are within 10% of one another, and only 3 rather weak lines have deviations worse than 20%. A similar comparison with the data from Froese Fischer et al. (2006) is given in Fig. 7. Unfortunately, in this case, the deviations are much larger,  $> 20\%$  or even 30% for a large fraction of the lines. Since the radiative M1 transition operator does not depend on the variable  $r$ , the main cause for the large deviations is that different CI expansion bases are used in our

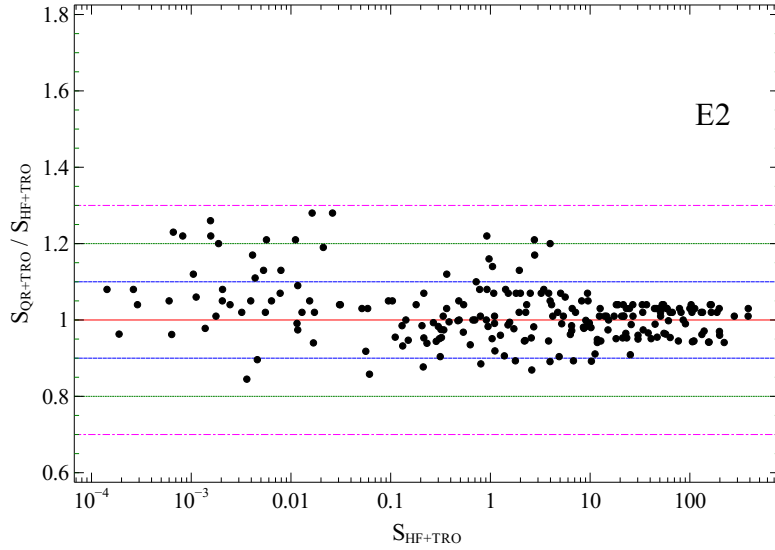


Fig. 4.— Comparison of the E2 transition line strengths  $S$  determined in the  $\text{CI}_{\text{HF+TRO}}$  and  $\text{CI}_{\text{QR+TRO}}$  approaches for S II.

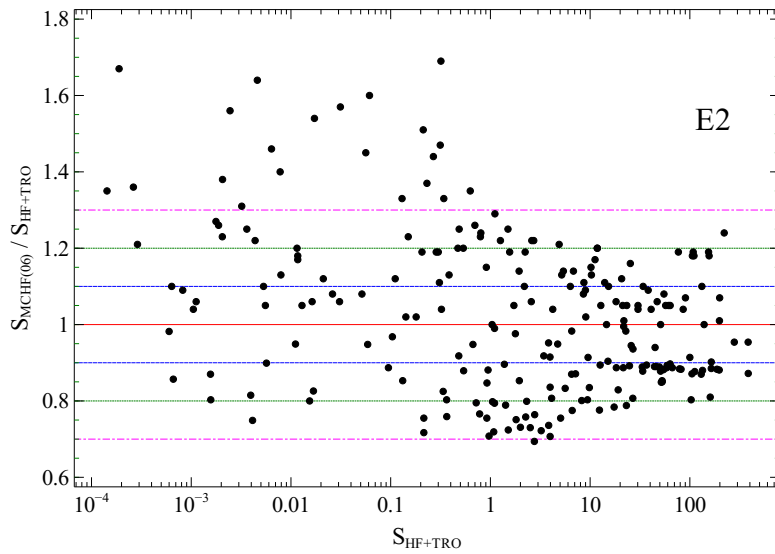


Fig. 5.— Comparison of the E2 transition line strengths  $S$  determined in the  $\text{CI}_{\text{HF+TRO}}$  and MCHF<sub>06</sub> (Froese Fischer et al. 2006) approaches for S II.

calculation and in the calculation by Froese Fischer et al. (2006).

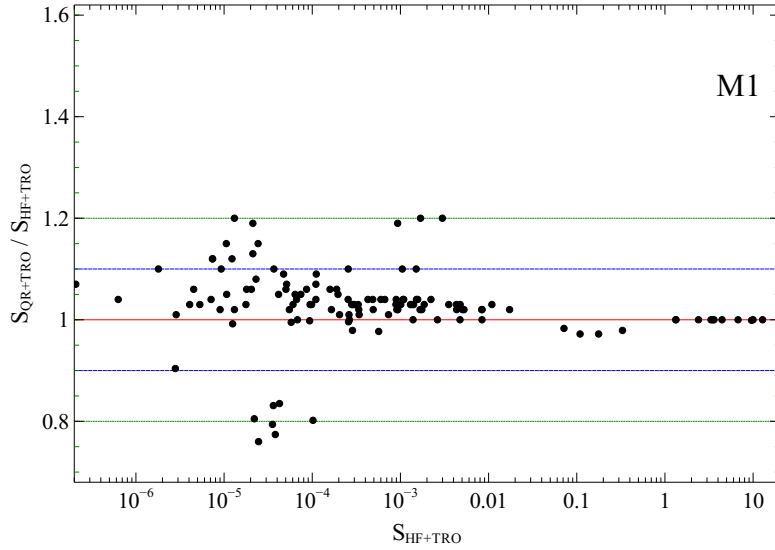


Fig. 6.— Comparison of the M1 transition line strengths  $S$  determined in the  $CI_{HF+TRO}$  and  $MCHF_{06}$  (Froese Fischer et al. 2006) approaches for S II.

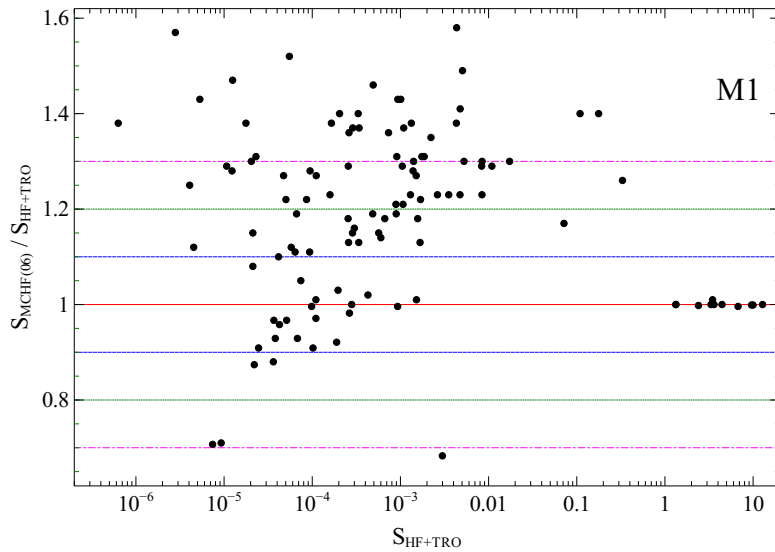


Fig. 7.— Comparison of the M1 transition line strengths  $S$  determined in  $CI_{HF+TRO}$  and  $MCHF_{06}$  (Froese Fischer et al. 2006) approaches for S II. Froese Fischer et al. (2006) approaches for S II.

## 4. Cloudy calculations

We have converted the new data to the STOUT format, the data base introduced in version 13 of Cloudy, the spectral synthesis code last described by Ferland et al. (2013). As described by Lykins et al. (2013a,b) and Ferland et al. (2013), Cloudy obtains much of its atomic and molecular data from external files, making it far easier to update and modify the data. For S II we combine our new calculations of the transition rates with NIST energy levels and collision strengths given by Tayal & Zatsarinny (2010). We save line strengths  $S$  rather than  $A_{ul}$  or  $gf$  because we use experimental energies –  $S$ , unlike the other two, does not depend directly on transition energy.

Table 3 lists a few of the calculated transition line strengths  $S$ ; the majority are available in the on-line version. The level indices are from Table 1, and the experimental level energies given there can be used to derive line wavelengths. These data were produced in the  $\text{CI}_{\text{HF}+\text{TRO}}$  approximation. Based on the listed data, one can easily transform transition line strengths  $S$  into the  $gf$  values or the transition rates  $A$  by using available experimental or calculated transition energies. Further details are given in Lykins et al. (2013b).

The following sections show representative sulphur spectra and discuss an application to DLAs.

### 4.1. Pure-S<sup>+</sup> emission spectra

Lykins et al. (2013a) describe our calculation of gas in collisional ionization equilibrium. We show two representative spectra, of absorption and emission spectra, in this section.

Two emission spectra of a pure-S gas in coronal equilibrium at  $T = 2 \times 10^4$  K, the temperature where the fraction of S<sup>+</sup> peaks, is shown in Figure 8. Both simulations have a

Table 3. Transition line strengths  $S$  (in a.u.) for S II determined in the  $\text{CI}_{\text{HF+TRO}}$  approximation.

Data	Type	$N_l$	$N_u$	$S$
S	E2	1	2	5.54E–03
S	M1	1	2	1.77E–05
S	E2	1	3	1.29E–02
S	M1	1	3	6.30E–07
S	E2	1	4	2.25E–06
S	M1	1	4	3.37E–04
S	E2	1	5	3.00E–10
S	M1	1	5	1.67E–03
S	E1	1	6	2.65E–01
S	E1	1	7	1.74E–01
S	M1	2	3	2.40E+00
S	E2	2	4	2.18E+01
S	M1	2	4	2.63E–03
S	E2	2	5	2.17E+01
S	M1	2	5	8.41E–03

Note. — The first column describes the transition data type (S stands for line strengths  $S$ , A – for transition rates  $A$ ). The second columns describes line type,  $N_l$  is for the lower level index,  $N_u$  denotes the upper level index.

Note. — (This table is available in its entirety in a machine-readable form in the online journal. A portion is shown here for guidance regarding its form and content.)

unit volume ( $1 \text{ cm}^{-3}$ ) of gas but have different densities,  $1 \text{ cm}^{-3}$  and  $10^{10} \text{ cm}^{-3}$ . The lower density is in the low-density limit and the spectrum would be characteristic of any gas with density  $n_e \lesssim 10^3 \text{ cm}^{-3}$ . As expected, the denser gas is  $\sim 10^{20}$  times more emissive. The higher density is characteristic of quasar emission-line regions (Osterbrock & Ferland 2006). The prominent feature at  $1197\text{\AA}$  is the  $\text{S}^+ \rightarrow \text{S}^0$  radiative recombination continuum. Many hundreds of S II lines are present, providing valuable diagnostics of the gas conditions.

The strongest lines in the lower density, upper panel of Figure 8, are the optical forbidden [S II]  $\lambda\lambda 6730.82, 6716.44$  doublet, a density indicator in nebulae (Osterbrock & Ferland 2006). The next strongest lines are the optical [S II]  $\lambda\lambda 4068.60, 4076.35$  doublet, which, combined with the previous pair, are a temperature indicator. Multiplets in the NIR at  $\lambda\lambda 10320, 10336, 10287, 10370$ , and in the FUV at  $\lambda\lambda 1259.52, 1253.81, 1250.58$ , are also strong.

The optical and NIR forbidden lines are collisionally suppressed in the denser gas shown in the lower panel. The strongest lines in this case are in the FUV, at  $\lambda\lambda 1259.52, 1253.81, 1250.58$  multiplet followed by  $\lambda\lambda 1204.32, 1204.27$ . These lines are allowed and are optically thick if the  $\text{S}^+$  column density is large enough.

## 4.2. Pure- $\text{S}^+$ absorption spectra

S II FUV lines are commonly observed in absorption in the interstellar and intergalactic media, and can be used to probe the composition of the intervening clouds. The lower panel of Figure 9 shows the absorption spectrum of a pure  $\text{S}^+$  gas with a column density of  $N(\text{S}^+) = 10^{15.2} \text{ cm}^{-2}$ . We consider models of DLA clouds in the following section, but present the absorption spectrum of a pure  $\text{S}^+$  gas here for completeness. The  $N(\text{S}^+)$  column density was chosen to be representative of the column density through the low-metallicity DLA clouds described in the next section. The Figure is limited to wavelengths  $\lambda > 1000\text{\AA}$

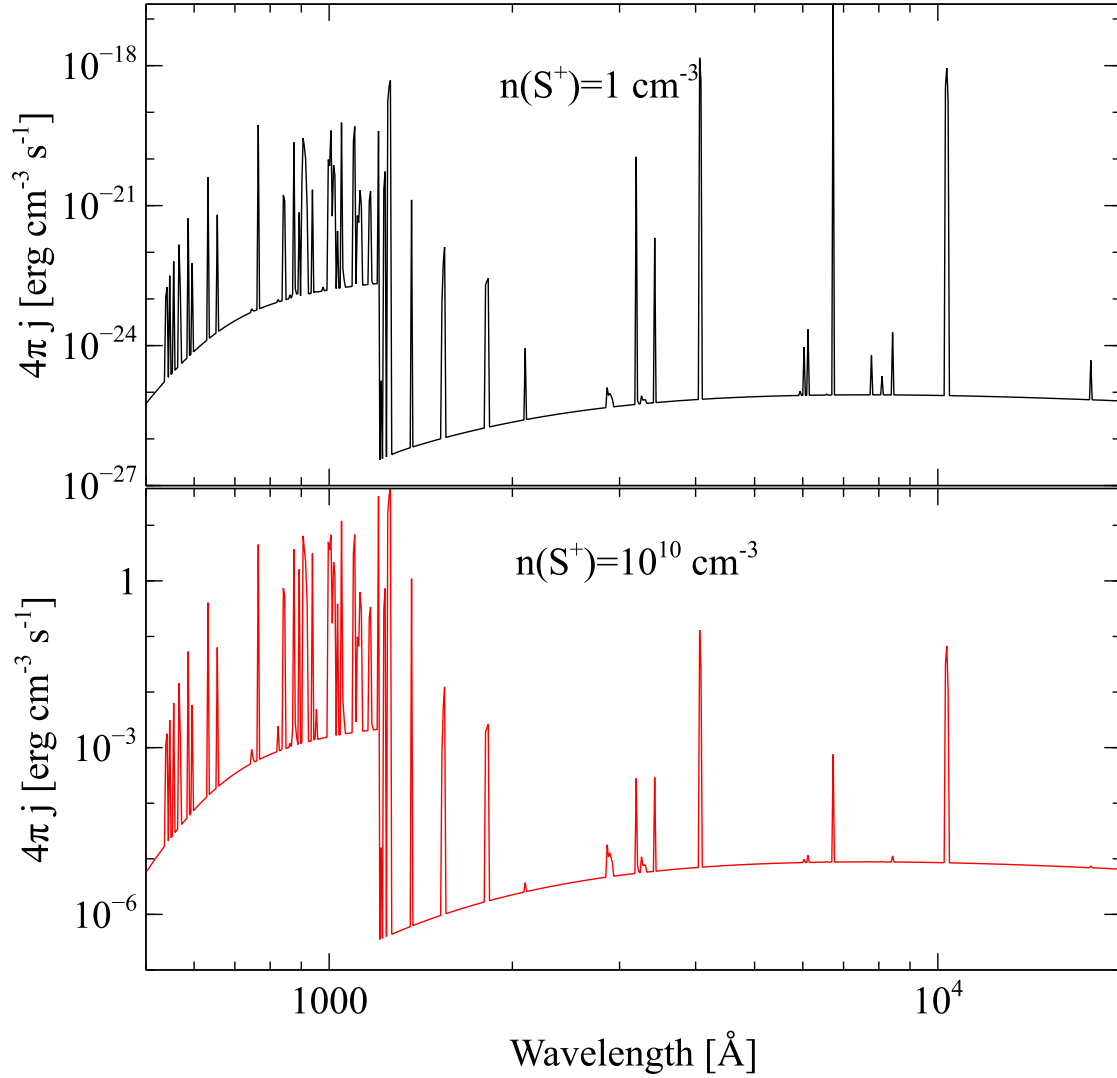


Fig. 8.— The S II emission spectra of a unit cell of pure-S<sup>+</sup> gas in coronal equilibrium at a temperature of  $2 \times 10^4$  K. Two S<sup>+</sup> densities,  $1 \text{ cm}^{-3}$  and  $10^{10} \text{ cm}^{-3}$  are shown. The low density produces a spectrum that peaks in the optical/NIR while the high density case emits mainly in the FUV.

since shorter regions are likely to be blocked by Lyman limit confusion.

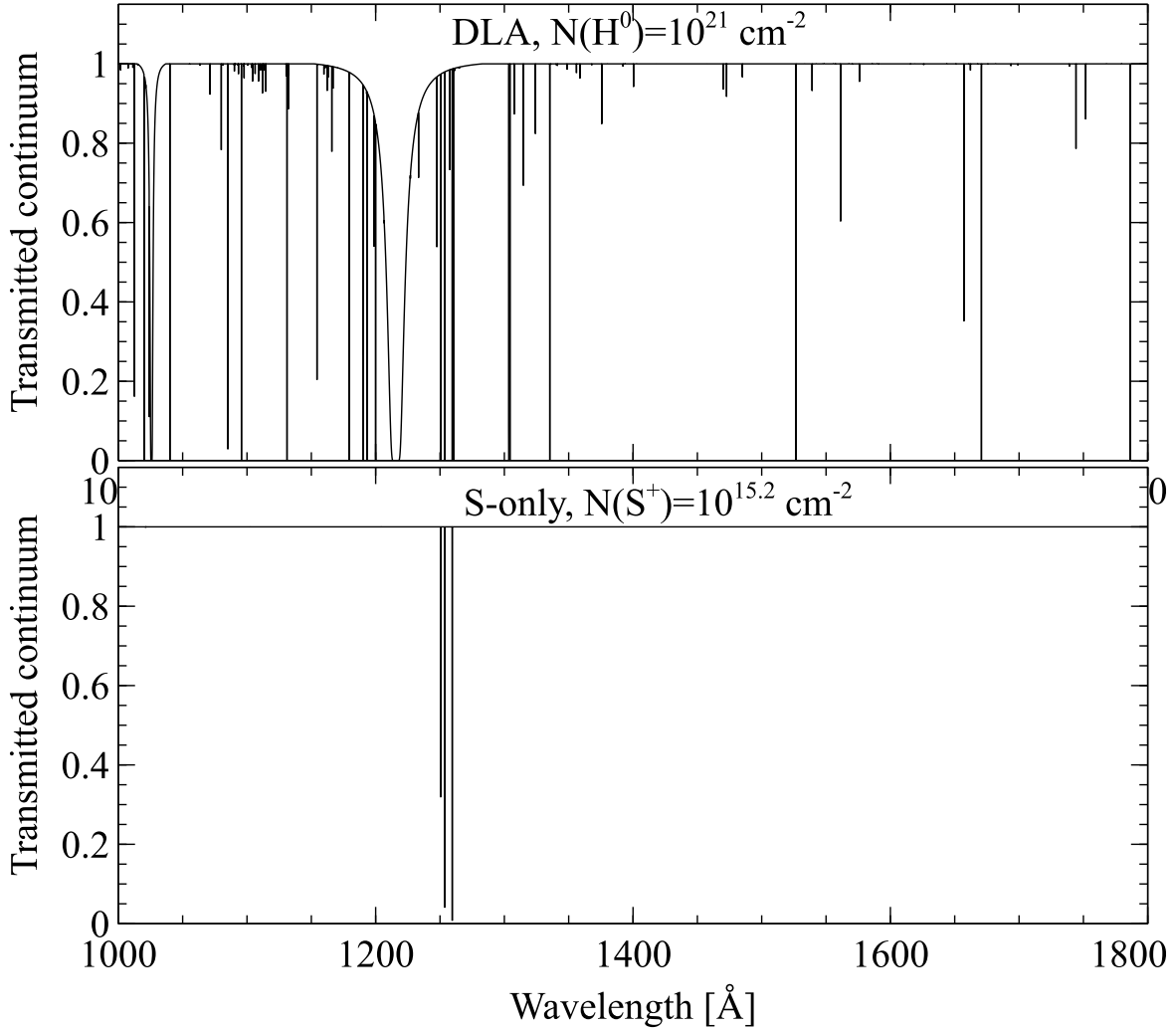


Fig. 9.— S II absorption plot. The upper panel shows a full DLA spectrum, with absorption lines of various elements shown relative to a normalized continuum. The strongest line is the damped Ly $\alpha$  line. The lower panel shows a spectrum in which all S is singly ionized. The  $S^+$  column density through the cell in the lower panel is similar to the  $S^+$  column density in the DLA shown in the upper panel.

Only a few S II lines (three lines near 1250 Å) are present in the spectral region shown in Figure 9. Other strong S II absorption lines are present, however. Table 4 lists

all predicted S II lines with optical depths greater than  $10^{-3}$ . Most of the lines are in the EUV, making them unobservable at cosmological distances; but we note that there are two multiplets near 1021 Å and 1204 Å which would be observable in higher column-density objects.

### 4.3. Application to DLAs

One aim of DLA absorption line spectroscopy is to be able to measure elemental abundances. In the case of S, we are often limited to the S II lines described in this paper. These can be used to infer the  $S^+$  column density, but to get abundances we must estimate the ionization fraction ratio  $S^+/S$ .

Howk & Sembach (1999) pointed out that certain ion ratios can be used to estimate ionization fractions of elements where only one stage of ionization is seen. We redo a calculation in the spirit of theirs. Like Howk & Sembach (1999), the SED is from Haardt & Madau (1996) and the total neutral hydrogen column density of the cloud is taken as  $N(H^0) = 10^{21} \text{ cm}^{-2}$ , roughly in the middle of the range of DLAs. We assume a redshift of  $z = 2$ . We assume ISM gas-phase abundances and dust with the metallicity and dust to gas ratio reduced by 1 dex, as is typical of these objects.

Given these assumptions, the only free parameter is the gas density. The metagalactic radiation background is assumed to be the only source of ionization. Given this SED the ionization of a DLA will be determined by its density, since the impinging flux of photons is constant. In this case, lower density gas will have a high ionization parameter (Osterbrock & Ferland 2006). The density range was chosen to cover the range of ionization parameters shown in Howk & Sembach (1999).

Figure 10 shows the results. The upper panel gives some observable ion ratios while the lower panel shows the computed  $S^+$  ionization fraction. Clouds with densities greater

than  $\sim 1 \text{ cm}^{-3}$  will have nearly all S in the form of  $\text{S}^+$ .

The full DLA spectrum of a cloud with a hydrogen density of  $1 \text{ cm}^{-3}$ , so that  $\text{S}^+$  is the dominant ion stage, and  $N(\text{H}^0) = 10^{21} \text{ cm}^{-2}$ , is shown in the upper panel of Figure 9. The  $\text{S}^+$  column density in the lower panel was chosen to be similar to the  $\text{S}^+$  column density through the DLA shown in the upper panel. These figures illustrate the potential of the new S II data for the purpose of making comparisons to observed spectra.

## 5. Discussion

Our oscillator strengths for most S II absorption lines agree closely with previous calculations. For example, for the triplet at 1250.6, 1253.8, and 1259.5 Å, our calculations are lower than previous ones by 0.04 dex. Thus, the metallicities inferred from these lines would be higher by 0.04 dex. It is reassuring that these metallicity corrections are relatively small.

One surprising result of our work is that the uncertainties NIST placed on the existing S II transition rates were too pessimistic. Their quality flags indicate a typical uncertainty of roughly 30%. Our independent calculations confirm the predictions of previous work, and suggest that the typical uncertainty is closer to 10% for the strongest lines.

Our Cloudy simulations illustrate an astrophysical application of the atomic data calculations, and the resultant predictions for a large number of emission and absorption lines. Such predictions can be compared with observed line strengths to better constrain the properties of distant galaxies. Past S II absorption line observations of DLAs have usually focussed on the strong lines at  $\lambda\lambda 1250.58, 1253.81, 1259.52$ . Our calculations confirm that these are the strongest lines in the observable part of the spectrum. Our full S II dataset posted online contains many UV transitions, some of which could be detected in high-S/N spectra with future large telescopes.

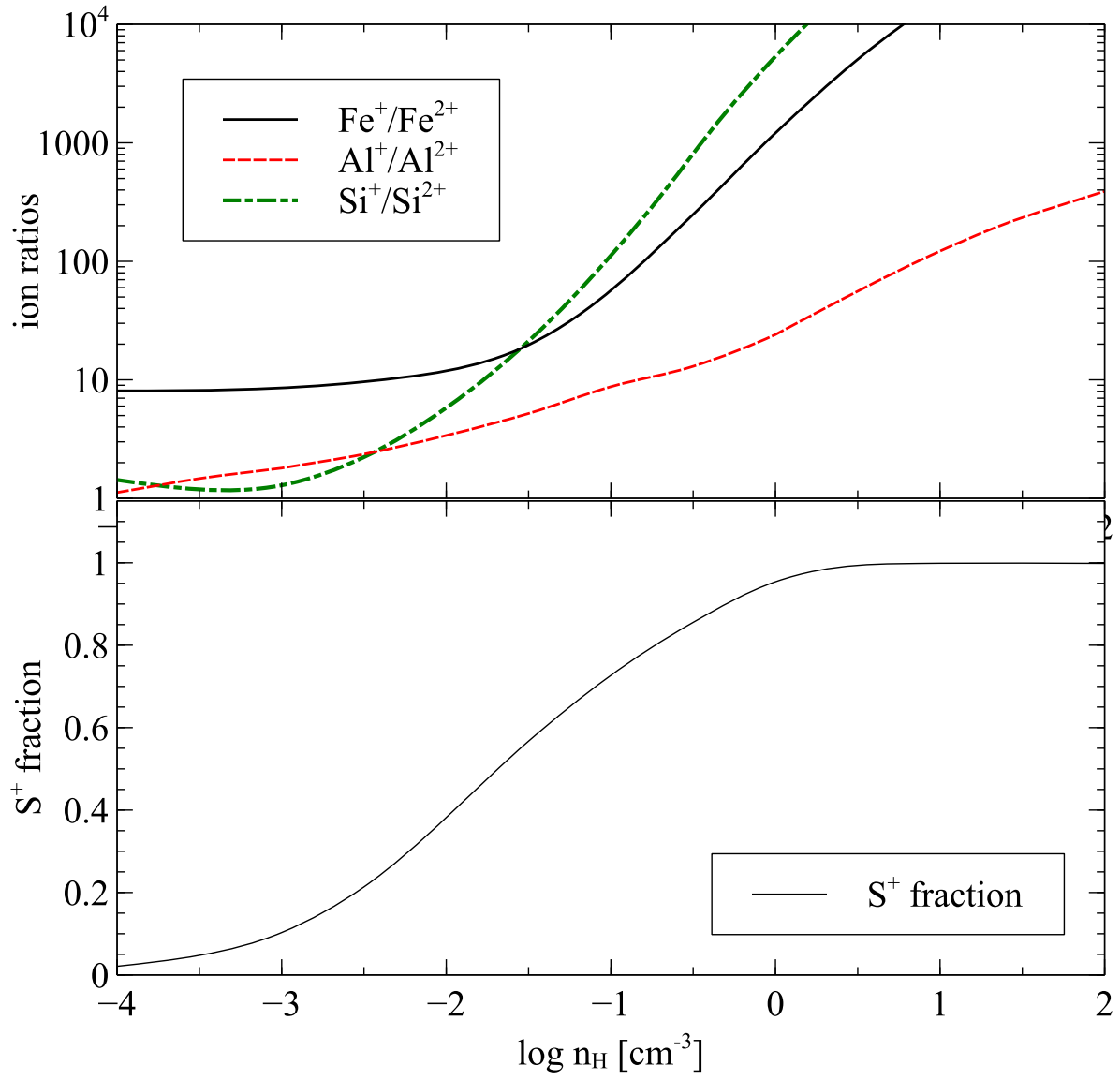


Fig. 10.— The upper panel shows the ratios of several commonly observed ions. The lower panel shows the predicted  $\text{S}^+$  ionization fraction. Several ratios correlate with  $\text{S}^+$  and can be used to estimate it.

It is also important to estimate how much difference to the true [S/H] can be caused by ionization effects. Our Cloudy calculations in Fig. 10 indicate that the ionization correction for [S/H] derived from S II / H I is small for typical DLAs. We note, however, that these calculations are subject to uncertainties in recombination coefficients. We plan to perform improved calculations of recombination coefficients in another part of this study.

We also note that theoretically calculated transition wavelengths can never reach the accuracy of experimental data. As is the standard practice in this field, we use experimental  $\lambda$  values in our Cloudy simulation runs. Transition probabilities or oscillator strengths must be corrected for the difference between experimental and theoretical energies, which is why our calculations work in terms of the line strength  $S$ . We do correct our transition rates by introducing the experimental level energies to determine radiative transition parameters, such as oscillator strengths  $gf$  or transition probabilities  $A$ , or tabulated data.

This paper is a demonstration of the work we plan to do for other ions of S as well as for the observationally important ions of other elements from Al to Zn. The results of these broader calculations will be presented in several future papers and made available to the astrophysics community through incorporation into Cloudy.

This work is supported by the National Science Foundation grant AST/1109061 to Univ. of Kentucky and AST/1108830 to Univ. of South Carolina. VPK also acknowledges partial support from NSF (AST/0908890) and NASA (HST-GO-12536). GJF acknowledges additional support by NSF (AST/1108928), NASA (10-ATP10-0053, 10-ADAP10-0073, and NNX12AH73G), and STScI (HST-AR-12125.01, HST-AR- 13245, GO-12560, and HST-GO-12309). RK's and PB's research is partially funded the European Social Fund under the Global Grant measure, project VP1-3.1-ŠMM-07-K-02-013.

Table 4. S II mean optical depths for S<sup>+</sup>-absorbing cloud in Fig.9

Ion	$\lambda(\text{\AA})$	Mean optical depth
S II	538	1.18E+00
S II	538	9.32E+00
S II	541	1.39E+01
S II	542	1.71E+00
S II	546	2.22E+01
S II	547	2.61E+00
S II	554	3.86E+01
S II	555	4.29E+00
S II	566	7.60E+01
S II	569	7.81E+00
S II	587	1.81E+02
S II	595	1.71E+01
S II	632	6.12E+02
S II	654	6.77E+01
S II	750	3.27E+03
S II	888	6.25E+02
S II	910	2.35E+02
S II	912	1.17E+02
S II	1021	1.50E−02
S II	1021	1.56E−03
S II	1204	1.34E−03
S II	1250	1.21E+01
S II	1253	2.44E+01
S II	1259	3.72E+01

## REFERENCES

- Battisti, A. J., et al. 2012, ApJ, 744, 93
- Bogdanovich, P. 2004, Lithuanian J. Physics, 44, 135
- Bogdanovich, P. 2005, Nuclear Instr. Meth. B, 235, 92
- Bogdanovich, P., Karpuškienė, R. 2001, Comput. Phys. Commun., 134, 321
- Bogdanovich, P., Karpuškienė, R., Momkauskaitė, A. 2002, Comput. Phys. Commun., 143, 174.
- Bogdanovich, P., Karpuškienė, R., Martinson, I. 2003, Phys. Scripta, 67, 44.
- Bogdanovich, P., Kisielius, R. 2012, At. Data Nucl. Data Tables, 98, 557
- Bogdanovich, P., Kisielius, R. 2013, At. Data Nucl. Data Tables, 99, 580
- Bogdanovich, P., Rancova, O. 2006, Phys. Rev. A, 052501
- Bogdanovich, P., Rancova, O. 2007, Phys. Rev. A, 012507
- Bogdanovich, P., Rancova, O. 2007, Phys. Scripta, 045301
- Chen, H.-W., Prochaska, J. X., Bloom, J. S., & Thompson, I. B. 2005, ApJ, 634, L25
- Cooke, R., Pettini, M., Steidel, C. C., Rudie, G. C., & Nissen, P. E. 2011, MNRAS, 417, 1534
- Cowan, R. D. *The Theory of Atomic Structure and Spectra* University of California Press, Los Angeles, 1981
- Ferland, G. J., Porter, R. L., van Hoof, P. A. M., Williams, R. J. R., Abel, N. P., Lykins, M. L., Shaw, G., Henney W. J., Stancil, P. C. 2013, Rev. Mexicana Astron. Astrofis., 49, 1 [<http://adsabs.harvard.edu/abs/2013RMxAA..49....1F>]

- Fritzsche, S., Fricke, B., Geschke, D., Heitman, A., Sienkiewicz, J. E. 1999, *ApJ*, 518, 994
- Froese Fischer, C., Tachiev, G., Irimia, A. 2006, *At. Data Nucl. Data Tables*, 92, 607
- Fynbo, J. P. U., Jakobsson, P., Prochaska, J. X., et al. 2009, *ApJS*, 185, 526
- Guimaraes, R., Noterdaeme, P., Petitjean, P., Ledoux, C., Srianand, R., Lopez, S.,  
Rahmani, H. 2012, *AJ*, 143, 147
- Haardt, F., & Madau, P. 1996, *ApJ*, 461, 20
- Howk, J. C., Sembach, K. R. 1999, *ApJ*, 523, L141
- Irimia, A., Froese Fischer, C. 2005, *Phys. Scripta*, 71, 172
- Jenkins, E. B. 2009, *ApJ*, 700, 1299
- Jonauskas, V., Bogdanovich, P., Keenan, F. P., Foord, M. E., Heeter, R. F., Rose, S. J.,  
Ferland, G. J., Kisielius, R., van Hoof, P. A. M., Norrington, P. H. 2005, *A&A*, 433,  
745
- Jonauskas, V., Bogdanovich, P., Keenan, F. P., Kisielius, R., Foord, M. E., Heeter, R. F.,  
Rose, S. J., Ferland G. J., Norrington, P. H. 2006, *A&A*, 455, 1157
- Jorgenson, R. A., Murphy, M. T., Thompson, R. 2013, *MNRAS*, 435, 482
- Karpuškienė, R., Bogdanovich, P. 2009, *At. Data Nucl. Data Tables*, 95, 533.
- Keenan, F. P., Hibbert, A., Ojha, P. C., Conlon, E.S. 1993, *Phys. Scripta*, 48, 129
- Kramida, A., Ralchenko, Y., Reader, J., and NIST ASD Team 2013, *NIST Atomic Spectra  
Database* (version 5.1), <http://physics.nist.gov/asd> National Institute of Standards  
and Technology, Gaithersburg, MD
- Kulkarni, V. P., Fall, S. M. 2002, *ApJ*, 580, 732

- Kulkarni, V. P., Khare, P., Proux, C., York, D. G., Lauroesch, J. T., Meiring, J. D. 2007, ApJ, 661, 88
- Kulkarni, V. P., Meiring, J., Som, D., Péroux, C., York, D. G., Khare, P., Lauroesch, J. T. 2012, ApJ, 749, 176
- Lykins, M. L., Ferland, G. J., Porter, R. L., van Hoof, P. A. M., Williams, R. J. R., Gnat, O. 2013a, MNRAS, 429, 3133
- Lykins, M. L., Ferland, G. J., Kisielius R., Porter, R. L., van Hoof, P. A. M., Williams, R. J. R. 2013b, in preparation
- Meiring, J. D., Kulkarni, V. P., Lauroesch, J. T., Proux, C., Khare, P., York, D. G., Crotts, A. P. S. 2009, MNRAS, 397, 2037
- Mendoza, C., Zeippen, C. J. 1982, MNRAS, 198, 127
- Morton, D. C. 2003, ApJS, 149, 205
- Osterbrock, D. E., Ferland, G.J. 2006, Astrophysics of Gaseous Nebulae & Active Galactic Nuclei, 2nd Ed. (Mill Valley; University Science Press) (AGN3)
- Péroux, C., Dessauges-Zavadsky, M., D’Odorico, S., et al. 2005, MNRAS, 363, 479
- Péroux, C., ., Meiring, J. D., Kulkarni, V. P., Khare, P., Lauroesch, J. T., Vladilo, G., York, D. G. 2008, MNRAS, 386, 2209
- Pettini, M., Smith, L. J., King, D. L., Hunstead, R. W. 1997, ApJ, 486, 665
- Podobedova, L. I., Kelleher, D. E., Wiese, W. L. 2009, J. Phys. Chem. Ref. Data, 38, 171
- Prochaska, J. X., Gawiser, E., Wolfe, A. M., Castro, S., Djorgovski, S. G. 2003, ApJ, 595,

- Prochaska, J. X., Herbert-Fort, S., Wolfe, A. M. 2005, *ApJ*, 635, 123
- Prochaska, J. X., Chen, H.-W., Dessauges-Zavadsky, M., et al. 2007a, *ApJ*, 666, 267
- Rafelski, M., Wolfe, A. M., Prochaska, J. X., Neeleman, M., Mendez, A. J. 2012, *ApJ*, 755, 89
- Savage, B. D., Sembach, K. R. 1996, *ARAA*, 34, 279
- Savaglio, S., Fall, S. M., Fiore, F. 2003, *ApJ*, 585, 638
- Som, D., Kulkarni, V. P., Meiring, J., York, D. G., Péroux, C., Khare, P., Lauroesch, J. T. 2013, *MNRAS*, in press (astro-ph/1307.7103)
- Storrie-Lombardi, L. J., Wolfe, A. M. 2000, *ApJ*, 543, 552
- Tayal, S. S., Zatsarinny, O. 2010, *ApJSS*, 188, 32.
- Verner, D. A., Verner, E. M., Ferland, G. J. 1996, *At. Data Nucl. Data Tables*, 64, 1